Gene Expression Tradeoffs Determine Bacterial Survival and Adaptation to Antibiotic Stress

Josiah C. Kratz [1,2] and Shiladitya Banerjee [3,*]

[1] *Computational Biology Department, Carnegie Mellon University, Pittsburgh, Pennsylvania 15213, USA*

[2] *Department of Biological Sciences, Carnegie Mellon University, Pittsburgh, Pennsylvania 15213, USA*

[3] *Department of Physics, Carnegie Mellon University, Pittsburgh, Pennsylvania 15213, USA*

(Received 17 October 2023; accepted 24 January 2024; published 29 February 2024)

To optimize their fitness, cells face the crucial task of efficiently responding to various stresses. This necessitates striking a balance between conserving resources for survival and allocating resources for growth and division. The fundamental principles governing these tradeoffs is an outstanding challenge in the physics of living systems. In this study, we introduce a coarse-grained theoretical framework for bacterial physiology that establishes a connection between the physiological state of cells and their survival outcomes in dynamic environments, particularly in the context of antibiotic exposure. Predicting bacterial survival responses to varying antibiotic doses proves challenging due to the profound influence of the physiological state on critical parameters, such as the minimum inhibitory concentration (MIC) and killing rates, even within an isogenic cell population. Our proposed theoretical model bridges the gap by linking extracellular antibiotic concentration and nutrient quality to intracellular damage accumulation and gene expression. This framework allows us to predict and explain the control of cellular growth rate, death rate, MIC, and survival fraction in a wide range of time-varying environments. Surprisingly, our model reveals that cell death is rarely due to antibiotic levels being above the maximum physiological limit, but instead survival is limited by the inability to alter gene expression sufficiently quickly to transition to a less susceptible physiological state. Moreover, bacteria tend to overexpress stress response genes at the expense of reduced growth, conferring greater protection against further antibiotic exposure. This strategy is in contrast to those employed in different nutrient environments, in which bacteria allocate resources to maximize growth rate. This highlights an important tradeoff between the cellular capacity for growth and the ability to survive antibiotic exposure.

DOI: 10.1103/PRXLife.2.013010

I. INTRODUCTION

Bacteria must regularly cope with a diverse set of harsh environments in their natural habitats. In unpredictable conditions, cells must balance the competing objectives of replication and protection against stress. Previous work has focused on identifying the molecular players, which control the bacterial stress response and understanding how specific genes confer protection against specific stressors [1–4]. In addition, the role of phenotypic heterogeneity and population-level bet hedging strategies in the bacterial stress response have been studied [2,5–7]. However, the fundamental principles governing the tradeoffs between expression of these genes and genes needed for growth is an outstanding question.

Antibiotic exposure is one such pertinent environmental stressor. Antibiotics are often produced by competing microbes [8,9], and are commonly used in the treatment of human infections [10]. Systems-level changes to bacterial physiology induced by antibiotic exposure, such as changes to cellular growth rate [11–14], gene expression [6,15–17], and cell morphology [18–21] have been well characterized. As a result, much is known about the proximate causes of antibiotic action, but vastly less is known about how these causes ultimately lead to bacterial cell death, and how cell death is abated by systems-level changes to cell physiology [22]. Furthermore, killing efficiency is not solely dependent on antibiotic dose, but on many other factors including the environment and the physiological state of the cell [Fig. 1(a)]. As such, to understand bacterial stress response strategies and to predict antibiotic efficacy in different environments, it is necessary to link environment not only to growth physiology, but also to damage accumulation and cell viability.

Previous work has shown that death rate increases approximately linearly with growth rate, but that the sensitivity of death rate to changes in growth rate depends significantly on environment and metabolic state [17,23–25]. Many mathematical models have been developed to link antibiotic dose to growth rate [13,26–28], but little has been done to connect growth physiology mechanistically to cell survival outcome. A recent work [17] identified a general stress-response sector in *E. coli*, whose expression reduces death rate. However, many questions remain unanswered: how is resource allocation to stress protein production mechanistically linked to the environment, and what specific effects does it have on cell physiology to mitigate antibiotic-induced death?

*Corresponding author: shiladtb@andrew.cmu.edu

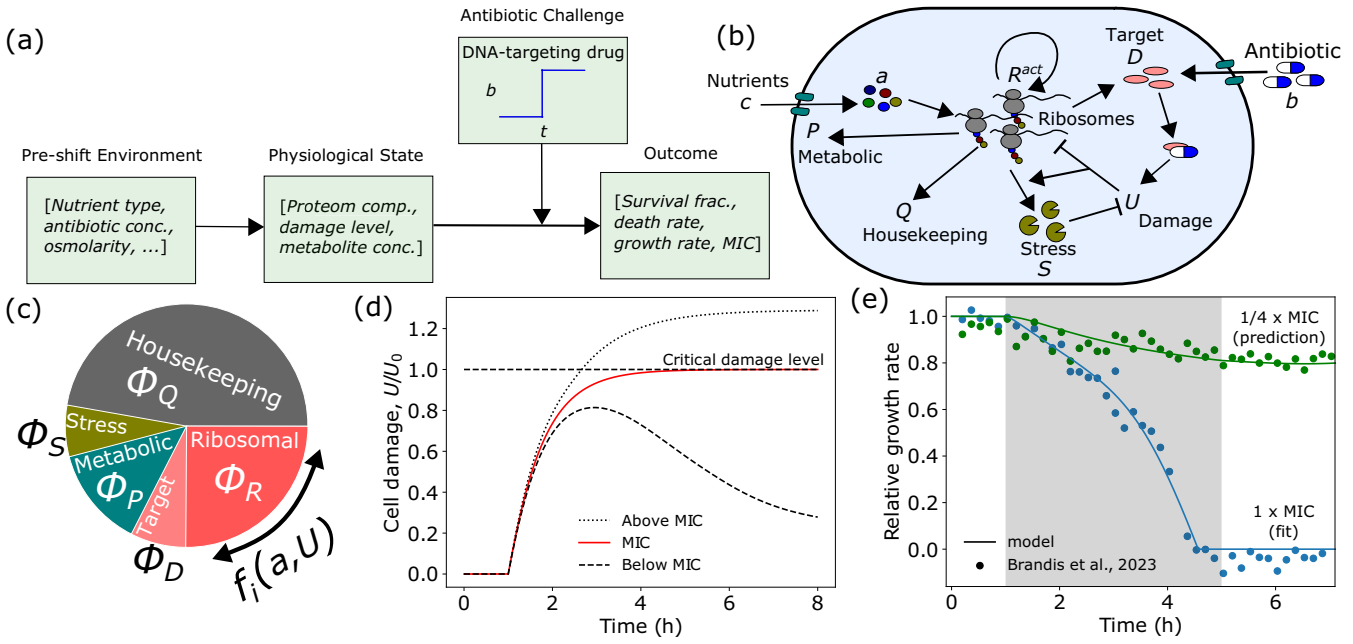

FIG. 1. Coarse-grained model for cell growth and death in dynamic antibiotic environments. (a) The survival outcome of a bacterial population exposed to antibiotics is heavily dependent on the preshift environment through its influence on the physiological state of the cell. (b) Schematic of coarse-grained model of bacterial physiology. Nutrients (c) are imported by metabolic proteins (P) and converted to amino acids (a), which are then consumed by ribosomes (R) to produce proteins. Antibiotics (b) enter the cell and bind their intracellular target (D) to produce damage, which can be repaired by stress proteins (S). (c) By dynamically regulating the fraction of the total translational flux devoted to each proteome sector i, f_i, in response to changes in a and U triggered by environmental changes, the cell alters its proteome composition, thus altering its susceptibility to further antibiotic challenge. (d) In our model framework, the minimum inhibitory concentration (MIC) is defined as the minimum value of b which causes U to cross the critical damage threshold ($U = U_0$). (e) Model successfully explains antibiotic-induced growth reductions for different values of b. Gray region indicates antibiotic application. Experimental data are of *E. coli* BW25993 cells in LB exposed to 8 (green) and 32 (blue) μg/ml of ciprofloxacin from Ref. [14] (see Fig. S3 [29] for data analysis details). See Table I for a list of model parameters, and Fig. S5 [29] for the effects of parameter variations on growth rate dynamics.

To gain a systems-level understanding of how cellular stress response and growth are connected to the environment and antibiotic killing efficiency, we have developed a multiscale model for cell growth and death, which coarse grains cellular physiology into a limited number of state variables and kinetic parameters to predict both single-cell and population-level behavior. Specifically, our model connects extracellular antibiotic concentration and nutrient quality to the stochastic dynamics of damage accumulation and proteome allocation to predict bacterial growth rate, death rate, and survival fraction in a wide range of time-varying environments.

We apply our model to predict changes in minimum inhibitory concentration (MIC) of antibiotics as a function of the environment in response to replication-targeting bactericidal antibiotics. We find that cells with reduced growth rates caused by stressful preshift environments are able to survive higher concentrations of antibiotics (increased MIC), in agreement with recent experimental data [17]. Our model predicts that this nonintuitive relationship between growth and death is a consequence of the dynamics of damage accumulation and removal, which are heavily dependent on the initial physiological state of the cell. Specifically, cells which are preexposed to low levels of antibiotics overexpress genes that can repair antibiotic-induced damage. Thus, when exposed to higher levels of antibiotics, they can more quickly repair new damage and survive, despite starting with an initially higher level of damage.

Our model predicts that there is a maximum antibiotic dose above which bacteria cannot survive unless through mutation, regardless of physiological state. However, model analysis reveals that cell death is rarely due to antibiotic levels reaching this limit, but instead survival is limited by the inability of a cell to alter gene expression sufficiently quickly to transition to a less susceptible physiological state. Our model highlights a critical gene expression tradeoff between growth and survival: allocation to stress response pathways is imperative to survive antibiotic challenge, but investment in these pathways reduces the resources available for growth. Thus, our model predicts that non-growth-optimal proteome allocation increases bacterial survival compared to growth-optimal allocation, a strategy which is preferred in many nutrient environments [30–32]. This tradeoff between allocation towards growth and stress response provides an explanation for the non-growth-optimal allocation observed in *E. coli* [11,15].

II. RESULTS

A. Resource allocation theory of cellular stress response in dynamic environments

Stress-induced cell death can be a consequence of many factors. For bactericides in particular, cell death is not

simply a result of target-specific inhibition. Instead, primary drug-target interactions perturb various metabolic pathways to induce an array of downstream effects, which can cause damage to both DNA and proteins [22,33–36]. To combat such damage, bacteria can induce both a nonspecific and specific stress response in which many similar proteins are upregulated in response to nutrient, antibiotic, or osmotic stress [17,35,37,38]. Bactericide-induced damage can be repaired by such proteins, e.g., SOS proteins in the case of DNA damage [1], allowing bacteria to survive and grow despite antibiotic challenge. Importantly, over short timescales survival is mediated by changes in gene expression, and is not due to genetic mutations [17,39].

Here we model physiological effects of bactericidal antibiotics, specifically those targeting DNA replication. Motivated by the common mechanism of cellular death induced by bactericides, we propose a coarse-grained model of damage accumulation and removal and connect it to cell physiology to predict bacterial growth and survival [Fig. 1(b)]. Specifically, the dynamics of the damage concentration U carried by a single cell can be expressed as

$$\frac{dU}{dt} = \alpha\phi_D b - \beta\phi_S U - U\kappa, \tag{1}$$

where b is the antibiotic concentration, which produces damage at a concentration specific rate α when bound to its target protein D, e.g., DNA gyrase in the case of quinolones [40]. Here ϕ_D represents the mass fraction of D, and U represents the total concentration of damage incurred by a single cell, which may include factors such as misfolded proteins, membrane and DNA damage, or other contributors to cell death. This coarse-grained approach to modeling cell damage has recently proved successful in the context of bacterial aging [41]. Damage is actively removed by stress proteins S, with mass fraction ϕ_S, at a rate β, and is also diluted with growth rate κ. Cell death occurs when damage accumulation exceeds a critical level U_0, such that $U(t = \tau_{\text{death}}) = U_0$. Mathematically, this threshold is the value of U above which the fixed point of the dynamical system, corresponding to survival, is no longer accessible in the deterministic model (discussed in more detail is Sec. II C). We assume that the dynamics of damage accumulation are much slower than the dynamics of antibiotic import and target binding, and thus model changes in b as instantaneous.

Critically, bacteria alter ϕ_S and ϕ_D in response to environmental changes. Thus, we connect damage accumulation dynamics to changes in gene expression following our recently introduced framework for dynamic proteome allocation [42]. In brief, cells import and convert nutrients to amino acids, with mass fraction a, via metabolic proteins, with protein mass fraction ϕ_P. Amino acids are consumed by translating ribosomes, with mass fraction ϕ_R, to synthesize all proteins, including themselves. As a result, ϕ_R sets the cellular growth rate, specifically $\kappa = \kappa_t(a, U)\phi_R$, where $\kappa_t(a, U)$ is the translational efficiency. Importantly, the translational efficiency is reduced under conditions of limited amino acid availability and elevated damage levels, in order to capture the effects of damage on the translational machinery (see Appendix A for details). The dynamics of each sector are given by

$$\frac{d\phi_i}{dt} = \kappa_t(a, U)\phi_R[f_i(a, U) - \phi_i], \tag{2}$$

where $i = [P, R, S, D, Q]$ and $f_i(a, U)$ denotes the fraction of total cellular protein synthesis flux devoted to sector i, and can be a function of a and/or U. We impose two constraints on the model motivated by *E. coli* proteomics data. First, a significant portion of the proteome is invariant to environmental perturbations [43], thus we define the housekeeping sector such that $\phi_Q = f_Q = \text{const.}$, and

$$\sum_{i\neq Q} f_i = 1 - f_Q = \phi_R^{\max}, \tag{3}$$

where $\phi_R^{\max}$ is the upper limit to the allocation fraction devoted to ribosomal proteins. Second, steady-state proteomics data [16] revealed that the molecular targets of many antibiotics, which inhibit DNA replication, such as DNA gyrases, are coregulated with ribosomal proteins under carbon, nitrogen, and translation limiting regimes (Fig. S1 [29]). As this work focuses on replication-targeting bactericides, we assume that the target sector, ϕ_D, is coregulated with the R sector, such that $\phi_D \propto \phi_R$. These constraints reduce the number of independent sectors to two, namely ϕ_R and ϕ_S.

Cells exhibit a general stress response, which is induced in response to cellular damage, and is mediated by various signaling molecules and transcription factors including ppGpp and RpoS [1,37,38,44,45]. Thus, f_S is indirectly activated by U, and we model its dependence by a simple sigmoidal function, $f_S(U) = \phi_S^{\max} U^2/(K_U^2 + U^2)$, where expression saturates at $\phi_S^{\max}$ and K_U is a constant. Additionally, steady-state transcriptomic analysis revealed that ribosomal sector expression is reduced to allow for stress sector expression [17]. As such, the fraction of total synthesis capacity devoted to ribosomes, f_R, is now a function of both a and U, where the maximum value of f_R is reduced as U increases (see Appendix A for details). When $U = 0$, f_R is chosen to maximize translational flux at steady state, thus maximizing growth rate [42,46,47].

Lastly, the dynamics of the amino acid mass fraction are given by the difference in the metabolic and translational fluxes, specifically

$$\frac{da}{dt} = \kappa_n(a)\left(\phi_R^{\max} - \phi_R - \phi_S - \phi_D\right) - \kappa_t(a, U)\phi_R. \tag{4}$$

Our model now has two key kinetic variables: a and U [Fig. 1(c)]. a acts as a readout of flux imbalance, driving metabolic and ribosomal proteome reallocation in response to nutrient changes. Increase in U caused by antibiotic application drives stress protein expression, which in turn can impact allocation to the other sectors.

Predicting minimum inhibitory concentration. Our model can be utilized to predict the minimum inhibitory concentration (MIC), typically defined as the antibiotic concentration threshold beyond which a bacterial population can experience complete extinction, while concentrations below the MIC allow the population to persist [39,48]. Thus, for a given preshift environment, the MIC can be predicted using our framework by identifying the minimum postshift antibiotic concentration b, which results in cell damage accumulating to the critical

TABLE I. Model parameters. See Appendix A for more details.

Parameter	Description	Value	Figure number
$\phi_R^{\max}$	Maximum flux allocation to ribosome production [12]	0.55	All
a_t	Translation attenuation threshold [47]	10^{-4}	All
a_n	Feedback inhibition threshold [47]	10^{-3}	All
κ_t^0 (h^{-1})	Translational efficiency rate constant, strain specific, fitted	2.7	2–6
		3.5	1
κ_n^0 (h^{-1})	Nutritional efficiency rate constant, nutrient specific, calculated	5.5	2–6
		1.12	1
α/U_0 ($\frac{ml}{\mu g\, h}$)	Normalized damage production rate constant, nalidixic acid, fitted	1.54	2–4, 5(d), 6
	Normalized damage production rate constant, ciprofloxacin, fitted	0.13	1, 5(a)–5(c)
β (h^{-1})	Damage removal rate constant, nalidixic acid, fitted	10.5	2–4, 5(d), 6
	Damage removal rate constant, ciprofloxacin, fitted	5.29	1, 5(a)–5(c)
K_u	Value of half-maximal expression, strain specific, fitted	0.076	2–6
		0.030	1
$\phi_S^{\max}$	Maximum flux allocation to stress protein production, antibiotic specific, fitted	0.33	2–4, 5(d), 6
		0.18	1, 5(a)–5(c)
σ	Noise amplitude, fitted	0.015	5, 6
μ_X (h^{-1})	Division protein degradation rate [42]	0.6	5, 6
γ_α (μm^{-3})	Division protein production parameter [42]	4.5	5, 6
γ_β (μm^{-3})	Division protein production parameter [42]	1.1	5, 6

threshold, $U(t) = U_0$ [Fig. 1(d)], which corresponds to cell death. This value can be obtained by solving the constrained optimization problem:

$$\text{MIC} \equiv \min b \;\; \text{s.t.} \;\; \max \mathbf{U} \geqslant U_0, \tag{5}$$

where $\mathbf{U}$ denotes the vector of damage values across time (see Appendix B for more details).

Taken together, Eqs. (1)–(4) define our model. This model can be fit well to experimental data (see Table I for a list of parameters), and yields extremely accurate predictions for growth rate dynamics for other antibiotic concentrations above and below the MIC not used in fitting (Fig. 1(e) and Fig. S2(a) [29]). Critically, when antibiotics are removed, growth rate recovers to its preshift value for antibiotic concentrations below the MIC, but does not recover for concentrations above the MIC (Fig. S2(b) [29]).

B. Growth rate control under stress

Bacteria must quickly alter gene expression to adapt to environmental stress. Our model can be utilized to predict the dynamics of damage accumulation, proteome allocation, and growth rate in response to time-varying antibiotic stress [Fig. 2(a)]. Antibiotic application leads to accumulation of damage, causing a sharp increase in allocation to stress protein production. Allocation to stress proteins largely comes at the expense of ribosomal allocation. This reduction in ϕ_R, in combination with the increase in U, results in a growth rate reduction [Fig. 2(a)].

Furthermore, the model is able to qualitatively capture experimentally observed [17] relationships between proteome allocation and growth rate across both nutrient and antibiotic conditions. Specifically, the model predicts that ribosomal sector allocation decreases with growth rate when growth is reduced either through a reduction in nutrient quality or through an increase in antibiotic concentration [Fig. 2(b)]. In contrast, stress sector expression is not affected by changes to nutrient quality, which reduce growth rate, but sector allocation increases with decreasing growth rate when growth is reduced by increasing the applied antibiotic concentration [Fig. 2(c)].

C. Effect of preshift environment on MIC

Interestingly, when comparing the relationship between preshift growth rate and MIC, the model predicts very different behavior based on the preshift environment [Fig. 3(a)]. Decreasing the growth rate by decreasing the nutrient quality has little impact on the MIC. However, decreasing the growth rate by exposure to low levels of preshift antibiotic result in significant increases in MIC, with higher preshift doses resulting in higher MIC values. These predictions quantitatively capture recent experimental results [17], and highlight the important role the environment plays in determining bacterial fitness in response to antibiotic challenge.

Our model predicts that these fitness gains by bacteria preexposed to antibiotics are explained by the differences in proteome allocation and their impact on the dynamics of damage accumulation. Cells in different nutrient environments initially do not carry damage, and so the stress sector is not expressed [Figs. 2(c) and 3(b)]. As a result, when antibiotics are applied, cells quickly accumulate damage regardless of initial growth rate, resulting in very similar values of MIC [Figs. 3(a) and 3(b)]. This can be seen in Eq. (1), where when ϕ_S is small, the dynamics of U are largely dictated by b (the smaller impact of ϕ_D will be discussed in later sections). In contrast, cells exposed to increasing initial levels of antibiotic both have increasing initial damage levels [Fig. 3(c)], but also have increased stress sector expression [Fig. 2(c)]. This yields the counterintuitive result that cells that initially have more damage are able to withstand higher antibiotic concentrations, resulting in an increased MIC

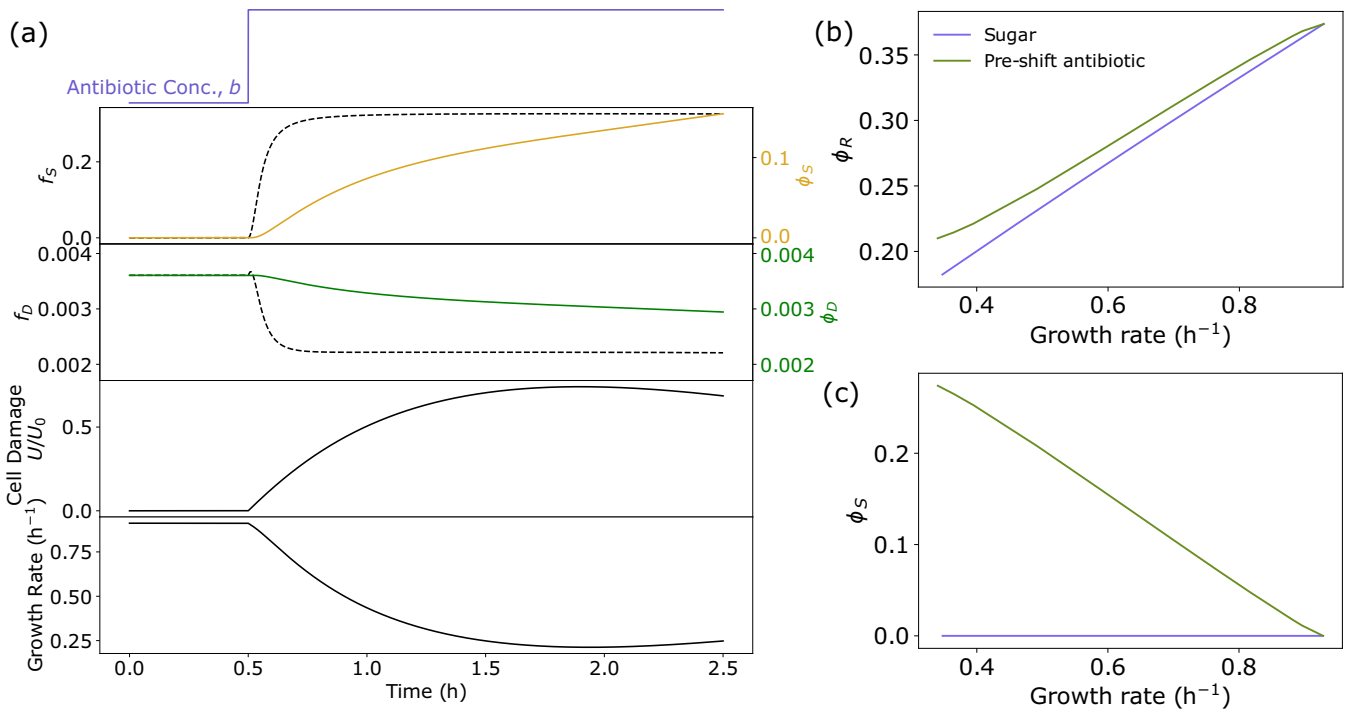

FIG. 2. Proteome reallocation and damage accumulation predicts bacterial growth rate across stress conditions. (a) Top to bottom: Antibiotic concentration, stress sector mass fraction, antibiotic target sector mass fraction, cell damage, and growth rate (κ) dynamics in response to stepwise application of replication-targeting bactericide at $t = 1$ h. (b), (c) Ribosome and stress sector mass fraction as a function of growth rate for different nutrient environments (blue) and for different concentrations of preshift antibiotic exposure (green). See Table I for a list of parameters.

[Figs. 3(a) and 3(c)]. Again this can be explained in terms of the dynamics of U: Slower-growing cells have higher initial values of ϕ_S, thus when additional antibiotics are applied, the damage removal rate is significantly higher, resulting in a higher value of b required for U to go above U_0.

An important prediction of this model is that the dynamics of damage accumulation and removal dictate survival, and that these dynamics are heavily influenced by the initial physiological state of a cell. Consequently, cell fate can be determined by considering a cell's position in the ϕ_S-U phase space immediately before an antibiotic shift. For most environments, there exists only one positive real steady-state solution of the system for a given antibiotic concentration, b, corresponding to a stable fixed point, which describes the steady-state physiology of surviving bacteria (growth bistability is predicted to occur only in very poor nutrient and high antibiotic environments, see Appendix C). Critically, this fixed point is not accessible from all regions of phase space. The trajectories of cells characterized by high damage levels and/or low stress sector expression will diverge away from the fixed point, resulting in cell death when $U = U_0$ [Fig. 3(d)]. Only cells with elevated values of ϕ_S and/or low values of U will have trajectories, which arrive at the fixed point, corresponding to survival [Fig. 3(d)].

Above a threshold antibiotic concentration $b_{\max}$, all fixed points become imaginary. This transition corresponds to the maximum survivable antibiotic concentration without mutation, and is given by $b_{\max} = \frac{\beta\phi_S^{\max}}{\alpha(\phi_R^{\max}(1+K_U^2)-\phi_S^{\max})}$. This value is much higher than concentrations typically required to cause cell death, as this fixed point is almost entirely inaccessible. Thus, our model reveals that cell death is rarely due to antibiotic levels being above the maximum physiological limit, but instead survival is limited by the inability to transition to the appropriate physiological state.

D. Non-growth-optimal resource allocation promotes bacterial survival

As shown in the previous section, a cell's survival is heavily dependent on the preshift environment, i.e., its initial position in the ϕ_S-U phase space. As a result, the specific way bacteria allocate resources in response to antibiotic exposure, and thus alter their position in ϕ_S-U space, has a significant impact on surviving additional increases in antibiotic level. For this reason, we were interested in comparing our proposed model to other potential resource allocation strategies. Bacteria are known to allocate resources to maximize growth rate in many different nutrient environments [30,46,47], and so we compared our model to the growth-optimal strategy.

The growth-optimal strategy was implemented by computing the growth-optimal proteome allocation [subject to the constraints of Eq. (3)] for each environment, using these values to set the allocation fractions $f_{i=[P,R,S,D]}$. Figure 4(a) shows stress protein expression as a function of damage level for both resource allocation strategies. Evidently, our proposed model significantly overexpresses stress proteins compared to the growth-optimal model for low and moderate damage levels. This result is consistent with experimental results

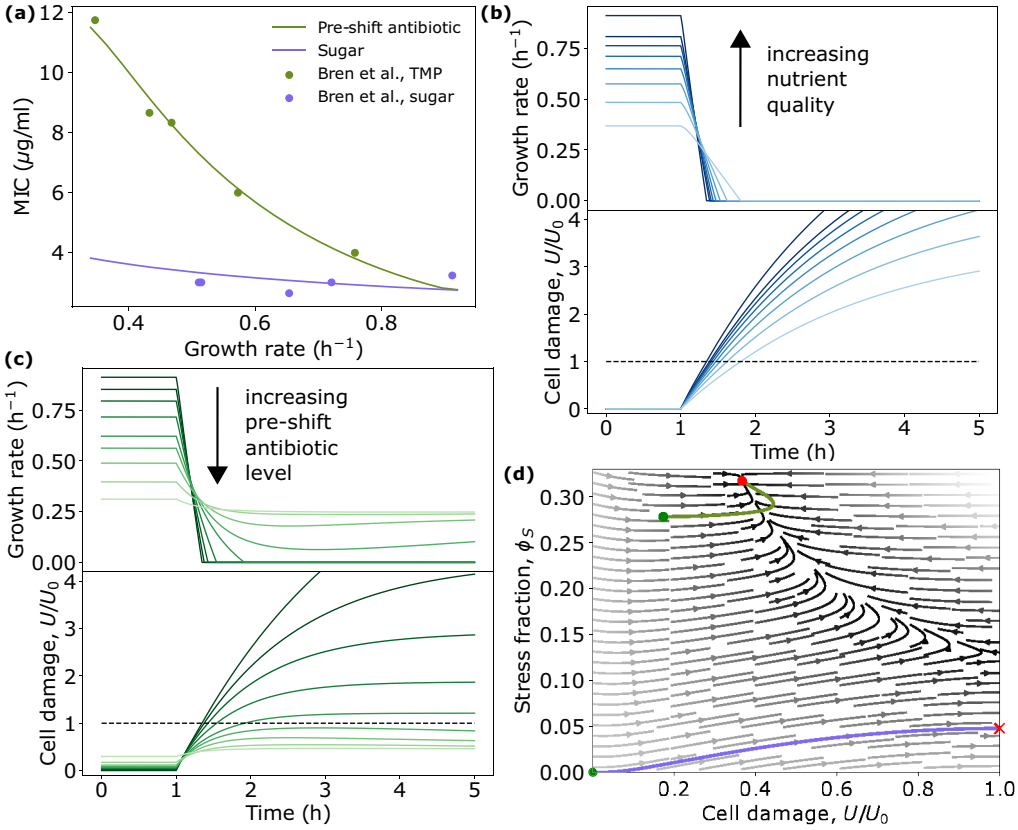

FIG. 3. Preshift environment heavily influences damage accumulation dynamics and survival. (a) Minimum inhibitory concentration (MIC) as a function of preshift growth rate under nutrient limitation (blue), and growth inhibition via low levels of preshift antibiotic (green), as computed from Eq. (5). Experimental data are from from Ref. [17] and are of *E. coli* NCM3722 cells grown in different sugars or exposed to different amounts of the bactericidal antibiotic TMP, before the MIC of nalidixic acid was measured. Model behavior is robust to parameter choice (see Fig. S6 [29]). (b), (c) Example trajectories of growth rate and damage accumulation for decreasing nutrient quality (b) and increasing preshift antibiotic concentration (c). (d) Phase portrait in ϕ_S-U plane with two example trajectories corresponding to preshift antibiotic exposure (green) and no exposure (blue). Green dots denote starting position, and red dot and X denotes fixed point and cell death, respectively. See Table I for a list of parameters.

showing that *E. coli* resource allocation is not growth-rate optimal when exposed to replication-targeting bactericides [11], but also raises the question, are there any potential fitness advantages conferred by this nonoptimal resource allocation strategy? To answer this, we computed the predicted MIC values for the growth-optimal strategy in a range of preshift antibiotic environments. In all environments tested, the MIC is significantly reduced compared to the non-growth-optimal model [Fig. 4(b)]. Thus, our model suggests that cells trade reduced growth for increased survival chances in bactericidal environments.

To understand how the overexpression of ϕ_S results in an increased MIC, we can again consider cell state dynamics in the ϕ_S-U phase space. With increasing antibiotic concentration b, the region in which the fixed point is accessible shrinks. Specifically, the boundary separating survival from cell death shifts upwards in the ϕ_S-U plane [Fig. 4(c)]. Thus, by overexpressing ϕ_S at low levels of b, cell survival becomes more resilient to further increases in b. Conversely, in the growth-optimal model, stress sector expression remains significantly lower for the same b value, positioning it much lower in the phase diagram. Here, even slight increments in b lead trajectories to be absorbed towards the boundary $U = U_0$ [see Fig. 4(c)], causing cell death.

E. Stochastic model of damage accumulation connects single-cell physiology to population-level behavior

Stress-induced cell death in an isogenic bacterial population is inherently stochastic [2,5]. When exposed to bactericidal antibiotics in particular, a significant fraction of bacteria die at sub-MIC concentrations, highlighting the stochastic nature of antibiotic killing. Furthermore, the fraction of surviving cells decreases in a dose-dependent manner [14,39]. Our deterministic theory is limited to binary outcomes, namely a population either entirely survives or is completely eradicated, and so is unable to capture these phenomena. Therefore, to explain population-level behavior induced by bactericides, we must include the effects of stochasticity on cell death. In our model, cell death is ultimately determined by damage accumulation to the threshold level. Many factors can contribute to stochasticity in this

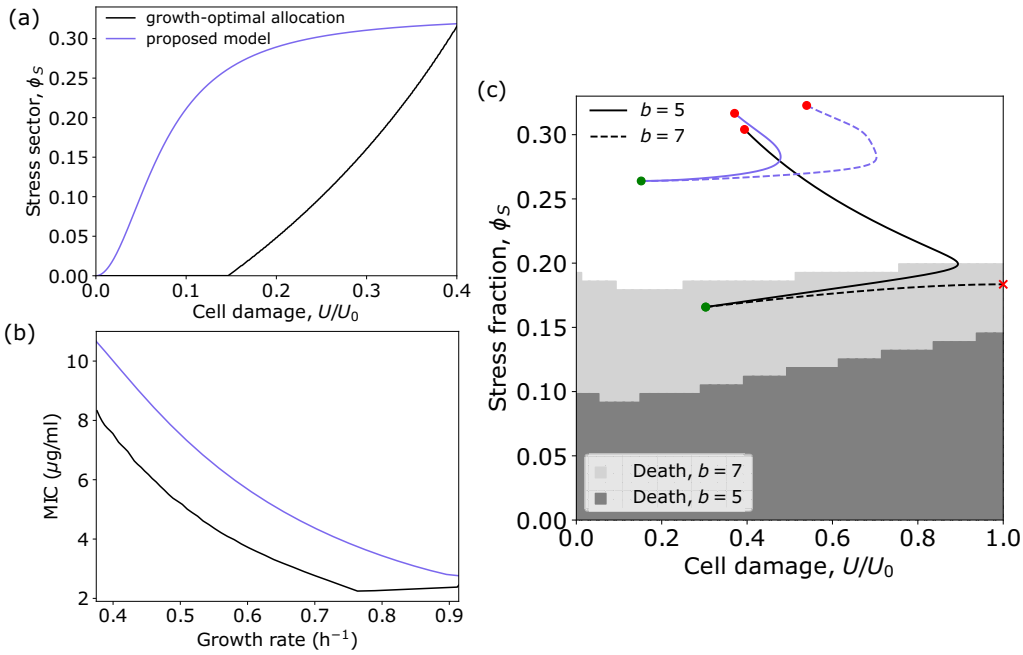

FIG. 4. Non-growth-optimal physiology increases bacterial survival. (a) Steady-state stress sector expression as a function of cellular damage for proposed model (blue) compared to growth-optimal allocation (black). For $U \leqslant 0.15$ growth-optimal allocation to stress protein expression remains at 0 because damage accumulation is prevented solely by growth dilution. (b) Predicted MIC for proposed model (blue) and growth-optimal allocation (black), with identical conditions as Fig. 3(a). (c) Cell outcome phase diagram for two values of b. Shaded regions indicate positions in phase space corresponding to cell death, whereas white indicates survival. Example trajectories from proposed model (blue) and growth optimal allocation (black), where dashed lines correspond to $b = 7$, and solid lines indicate $b = 5$. See Table I for a list of parameters.

process, including noise in gene expression, antibiotic import, and damage removal. As such, we choose to coarse grain the noise in damage accumulation and reformulate the deterministic dynamics of U in terms of a Langevin equation, yielding

$$dU_t = (\alpha\phi_D b - \beta\phi_S U_t - U_t\kappa)dt + \sqrt{2\sigma}dW_t, \qquad (6)$$

where W_t denotes a Wiener process with variance σ^2. Example trajectories using this framework are given in Fig. 5(a), and show that cell death can occur even when the deterministic trajectory remains well below the critical damage threshold. Importantly, as the average damage level approaches the threshold, smaller deviations away from the mean are required for a cell to die, thus increasing the probability of death. More formally, Eq. (6) can be written in terms of a potential function, and the risk of death and survival fraction can be approximated as a function of antibiotic concentration in our model from the first-passage time of U above U_0 (see Appendix D). Using the best-fit strain and antibiotic-specific parameters from the deterministic model, σ can be fit to yield good agreement between theory and data for experiments where survival fraction is not impacted by division rate [Fig. 5(b)].

Although our stochastic model can capture the decrease in survival fraction with increasing antibiotic concentration seen experimentally, it does not take into account replication of surviving bacteria. Thus, to fully capture population-level behavior, we must both model single-cell death and division dynamics, which requires adding rules for division. To this end, we add a new sector, X, which regulates cell reproduction using rules for division and proteome allocation from our previous work (detailed in Ref. [42]). This allows us to simulate populations of cells in complex time-varying environments, with population dynamics governed by single-cell death and division events.

Using this stochastic multiscale model, we simulated single-cell trajectories for a population of cells, tracking the total number of living and dead cells over time in response to antibiotic application [Fig. 5(c)]. We found a significant portion of the population died at antibiotic concentrations below the MIC due to stochastic damage accumulation above the critical threshold, while a surviving subpopulation continued to grow and divide, in agreement with experimental observations [14]. Importantly, once $U = U_0$ the cell dies and damage cannot return to the mean value. Thus this absorbing boundary condition allows for the creation of two stable subpopulations defined by cell viability.

We calculated the fraction of surviving cells after simulating different time intervals of antibiotic exposure for increasing sub-MIC antibiotic concentrations, using the previous best-fit parameters. Not surprisingly, shorter exposure resulted in a higher survival fraction, with survival fraction stabilizing after several hours of exposure [Fig. 5(b)]. The dependence of exposure time on survival fraction is antibiotic specific, because it is set by the dynamics of damage accumulation specific for each drug, thus highlighting the necessity of considering exposure time when assessing killing efficiency. The fraction of surviving cells decreased with increasing antibiotic concentration, however, the survival fraction was

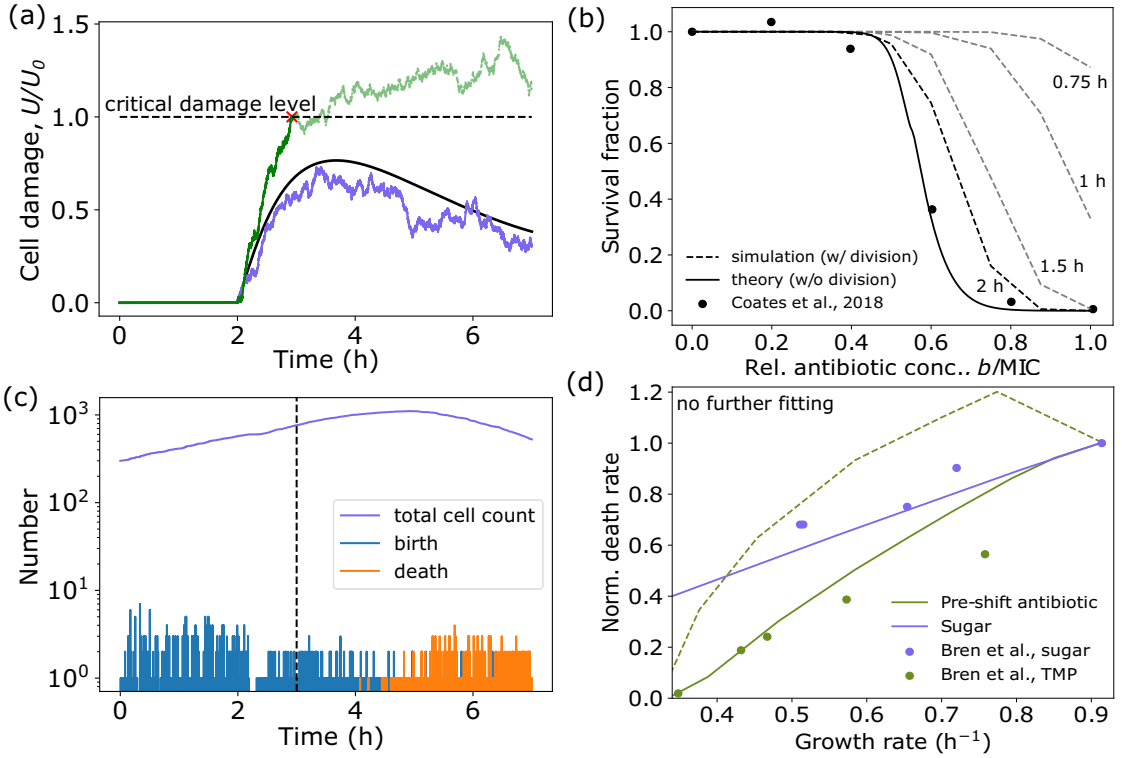

FIG. 5. Stochastic model captures population-level behavior. (a) Representative trajectories of cell damage in response to antibiotic application at $t = 2$ h. At sub-MIC concentrations, the deterministic dynamics (black) remain below $U = U_0$, but in the stochastic case, both survival outcomes are possible, with some cells surviving (blue) and others dying (green). (b) Survival fraction of a bacterial population exposed to various concentrations of antibiotic, relative to the MIC. Solid line denotes theoretical prediction from first-passage time of U above U_0, dotted lines denote population simulation results for different durations of antibiotic exposure. Experimental data are from Ref. [39] and are of *E. coli* NCM3722 cells in LB exposed to ciprofloxacin, determined via plating efficiency. Model behavior is robust to parameter choice (see Fig. S7 [29]). (c) Population dynamics for bacteria exposed to antibiotics at $t = 3$ (dashed line), initialized with 300 cells. Following a division event, both resulting daughter cells were simulated. For each cell if $U \geqslant U_0$, the cell was removed, corresponding to cell death. (d) Death rate of *E. coli* in 10 μg/ml nalidixic acid, defined as the inverse of the time required for 90% of the initial population (4000 cells) to be eliminated, as a function of preshift growth rate, normalized to the death rate in glucose. Solid lines indicate our proposed model, dashed line indicates growth-optimal resource allocation model. Data from Ref. [17]. See Table I for a list of parameters.

always greater than that predicted by the single-cell theory [Fig. 5(b)]. This is because sub-MIC, surviving cells are able to continue to grow and divide, thus inflating the number of living cells.

F. Population-level death rates are predicted by single-cell physiological state

To assess how the preshift environment and cellular stress response affects bacterial death dynamics, we used our multiscale model to simulate cell population dynamics in response to antibiotic exposure above the MIC. Here, to facilitate comparison with experimental data [17], we defined the death rate as the inverse of the time required for 90% of the initial population to be eliminated ($1/t_{90}$). Interestingly, in all cases death rate decreased with decreasing growth rate, with cells preexposed to low levels of antibiotic having a lower death rate than those in a poor nutrient environment with the same growth rate [Fig. 5(b)].

As with the predictions for the MIC, the reduction in death rate for cells preexposed to low levels of antibiotic is largely explained by the increase in stress protein expression causing a reduced rate of damage accumulation [Fig. 3(b)]. However, the decrease in death rate for cells in poor nutrient conditions is caused by a decrease in concentration of the antibiotic target, ϕ_D. This can be understood by considering Eq. (1) and bearing in mind that, since we are considering gyrase-targeting antibiotics, $\phi_D \propto \phi_R$, and ϕ_R decreases with decreasing nutrient-imposed growth rate [Fig. 2(b)]. Consequently, slower-growing cells produce less damage [Fig. 3(b)]. As all cells initially have no damage, and thus no stress protein expression, and cell division is greatly reduced in all cases regardless of nutrient quality, differences in damage production dominate the dynamics of damage accumulation, and thus death rate. Importantly, we also simulated death dynamics using the growth-optimal resource allocation strategy, and found that death rates were significantly higher for this allocation strategy compared to our proposed model, and did not match the experimental data [Fig. 5(d)]. In fact, death rate increases at low preshift antibiotic levels in the growth-optimal model, as cells in this regime initially carry more damage, but do not induce a stress response [Fig. 4(a)]. This further supports the notion that bacteria utilize a non-growth-optimal proteome allocation

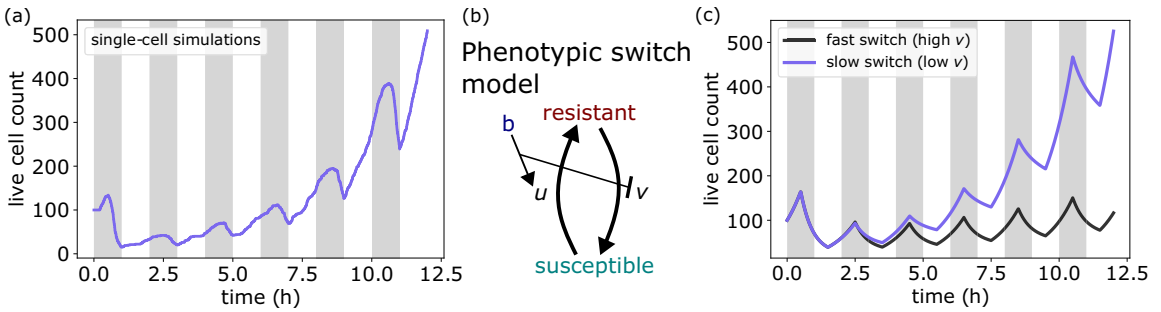

FIG. 6. Proteome reallocation confers mutation-independent adaptation. (a) Population dynamics from single-cell simulations for bacteria under pulsatile antibiotic exposure above the MIC, initialized with 100 cells. Population recovers and surpasses initial size after four pulses. See Table I for a list of parameters. (b) Schematic depicting phenotypic switch model for population dynamics in time-varying environment. In response to antibiotic application (b), susceptible cells alter their gene expression to become more resistant at rate u, at the cost of a reduced growth rate. Upon antibiotic removal, cells switch back at rate v. See Appendix E for more details. (c) Phenotypic switch model can capture the adaptation to pulsatile exposure seen in (a).

strategy in order to increase survival chances under antibiotic challenge.

G. Differing timescales of stress exposure and proteome reallocation enable mutation-independent adaptation

With our model able to capture experimentally observed growth rate, gene expression, and death dynamics, we then tested the model in more complex time-varying environments, focusing on pulsatile antibiotic exposure. We simulated a bacterial population growing in rich media subjected to repeated bactericide application. Interestingly, we found that for concentrations above the MIC of the initial population, population size recovered to its initial value after several pulses and then surpassed it as cells continued to proliferate [Fig. 6(a)].

These results identify a short-timescale, mutation-independent, adaptive response to bactericidal antibiotic exposure. Initially, antibiotic-induced damage accumulation occurs quickly, resulting in high rates of cell death. However, damage accumulation also causes bacteria to increase ϕ_S expression (Fig. S4 [29]). As a result, cells that survive the initial pulse are better able to withstand subsequent exposure, resulting in an increased MIC and decreased death rate amidst future antibiotic challenge. Importantly, when antibiotics are removed, bacteria again reallocate their proteome to maximize growth, resulting in a decrease in ϕ_S. Consequently, the observed adaptation is a result of the difference in timescales of antibiotic application and proteome reallocation. Specifically, when reallocation is slower than the time period of application, surviving cells will on average have a higher value of ϕ_S upon reexposure compared to cells one period prior. As a result, the physiological state of surviving cells is better able to combat the next round of antibiotic application, thus yielding a higher survival fraction, in agreement with experimental observations [49].

Simulations in time-varying environments again highlight the importance of the physiological state of the cell in determining antibiotic killing efficacy. In such environments, this altering of physiological state can be modeled as a phenotypic switch between two subpopulations [Fig. 6(b)], a framework that has been used successfully in pharmacodynamics (PD) to model resistance evolution [50], as well as in modeling bacterial persistence [6]. Critically, unlike previous work, here susceptibility is not altered via mutations or persister formation, but due to changes in gene expression (sector allocation) in growing cells (see Appendix E for full model description and Table II for a list of parameters). Using this framework, we constructed a population-level description of our multiscale model, which was able to reproduce the observed adaptive behavior [Fig. 6(c)]. Importantly, this adaptive behavior was mitigated when proteome reallocation after antibiotic removal was accelerated [Fig. 6(c)], demonstrating that slow phenotypic switching can facilitate adaptation to pulsatile environments.

III. DISCUSSION

We have developed a multiscale model for cell growth and death, which connects extracellular antibiotic concentration and nutrient quality to bacterial physiology, allowing us to quantitatively capture the observed control of growth rate, death rate, minimum inhibitory concentration (MIC), and survival fraction across a wide range of environments. Although the model has been derived based on data from *E. coli* under replication-targeting bactericides, we expect the theoretical framework of proteome allocation theory and damage

TABLE II. Model parameters for phenotypic switching model.

Parameter	Value
$\kappa_{\max}$	1
$\kappa_{\min}$	−10
n	2
c	0.25
MIC_S	1
MIC_R	2.15
$u_{\max}$	0.2
$v_{\max}^{\mathrm{high}}$	0.85
$v_{\max}^{\mathrm{low}}$	0.2

accumulation to generalize to other environmental stressors and other microorganisms. Using proteomics data in conjunction with MIC assays for a particular organism and drug pair, the various proteomic and kinetic parameters can be elucidated in our model, allowing for quantitative prediction of growth rate control and death rate in complex time-varying environments.

Our model reveals that cell death seldom occurs due to antibiotic levels exceeding the maximum physiological tolerance, but rather, cell survival hinges on the ability to transition to the appropriate physiological state. Consequently, the MIC of a bacterial population, typically assumed to remain constant unless raised by mutations [51], can be significantly altered by manipulating its physiological state through environmental changes. In addition, our model brings understanding to how changes in gene expression enable cellular adaptation in fluctuating environments. This is extremely pertinent over short timescales, when resistant mutations have yet to accumulate. As a result, our model has direct clinical relevance, as it allows for quantitative prediction and understanding of bacterial growth and death in time-varying nutrient and antibiotic environments at both the single-cell and population levels.

Furthermore, our model predicts that when exposed to bactericides, bacteria tend to overexpress stress response pathways at the expense of growth. This strategy enhances their resilience to future antibiotic challenge but comes at the cost of growth potential. This strategy highlights an important gene expression tradeoff that cells must make between growth and survival. Protection against environmental stress is expensive, as it requires synthesis of energy-consuming homeostatic mechanisms and repair processes [52]. Allocation towards such processes reduces the resources available for growth. Moreover, in fluctuating environments, rapid adaptation can confer a fitness advantage. As such, bacteria must continually respond to environmental changes to execute a program that balances the needs for both growth and survival.

Our modeling framework can easily be extended in future work to capture other environments and physiological contexts. The effects of dynamic stressors on drug-resistant bacteria, which constitute a serious global health problem [3,4], can be studied by adding an additional proteome sector corresponding to the expression of resistance-conferring genes, or by altering the effective damage removal rate constant (β). In addition, our framework could be used to study the complex and nonintuitive effects of antibiotic combinations [1,53,54]. As our model is able to predict growth and death dynamics, it is particularly well suited to investigate temporal interactions between sequentially applied drugs in order to understand the effects of antibiotic-induced phenotypic changes on future drug applications.

ACKNOWLEDGMENTS

S.B. acknowledges support from the National Institutes of Health (NIH R35 GM143042), and the Shurl and Kay Curci Foundation. J.C.K. and S.B. designed and developed the study. J.C.K. carried out the simulations and analyzed the data. J.C.K. and S.B. wrote the paper.

APPENDIX A: MODEL DERIVATION

To connect the physiological effects of bactericidal application to the population-level dynamics of cell death, we propose a coarse-grained process of damage accumulation and removal and connect it to other cell-level processes. Specifically, the dynamics of cell damage concentration U for a single cell can be expressed as $\frac{dU}{dt} = \alpha d b - \beta s U - U\kappa$, where b is the antibiotic concentration, which produces damage at a concentration specific rate α when bound to its target D, with concentration d. Damage is removed by stress proteins, with concentration s, at rate β, and is diluted by cell growth at rate κ. Cell death occurs when the damage level exceeds a critical concentration, $U(\tau_{\text{death}}) = U_0$. In many conditions, cell density remains constant and total protein mass is proportional to the cell's dry mass [55,56], thus the concentration of each protein sector i can equivalently be expressed in terms of mass fraction, ϕ_i. Therefore our equation for damage dynamics can be rewritten as

$$\frac{dU}{dt} = \alpha \phi_D b - \beta \phi_S U - U\kappa, \tag{A1}$$

where the constants α and β are now mass fraction specific rates.

A significant number of known bactericides target the DNA gyrase, thus preventing replication. Steady-state proteomics data revealed that DNA gyrases are coregulated with ribosomal proteins under carbon, nitrogen, and translation limiting regimes [16]. Thus we assume such coregulation is maintained under DNA gyrase antibiotic challenge, such that its proteome fraction, ϕ_D, is proportional to the R sector ($\phi_D = \nu \phi_R$). Therefore Eq. (A1) becomes $\frac{dU}{dt} = \tilde{\alpha} \phi_R b - \beta \phi_S U - U\kappa$ where $\tilde{\alpha} = \nu\alpha$.

Following our previous model for dynamic proteome allocation [42], we can connect damage dynamics to changes in gene expression. Specifically, stress sector dynamics are given by

$$\frac{d\phi_S}{dt} = \kappa_t(a, U)\phi_R[f_S(U) - \phi_S], \tag{A2}$$

where $f_S(U)$ is the fraction of total cellular protein synthesis flux devoted to stress proteins and κ_t denotes the translational efficiency. We assume stress protein expression is solely dependent on the damage amount, such that $f_S(U) = \phi_S^{\max} \frac{U^2}{K_U^2 + U^2}$. As before [42], κ_t is reduced by low levels of a. Importantly, κ_t is now also reduced by increases in U to capture the effects of damage on protein production. This reduction can be caused by direct inactivation of ribosomal proteins, as in the case of aminoglycosides [57], or be caused by indirect effects as is the case for quinolones, where DNA synthesis inhibition reduces protein production via a decrease in cellular DNA concentration [28]. Although we choose to model the effects of damage on growth through the translational efficiency, κ_t, this can equivalently be thought of as a growth reduction caused by inactivation of translating ribosomes, indeed this yields a mathematically equivalent expression. Thus, $\kappa_t(a, U) = \kappa_t^0 g(a)(1 - U/U_0)$ for $0 \leqslant U/U_0 \leqslant 1$, where the regulatory function $g(a)$ is defined below. Similarly to Eq. (A2), ribosomal sector dynamics

are given by

$$\frac{d\phi_R}{dt} = \kappa_t(a,U)\phi_R[f_R(a,U) - \phi_R]. \tag{A3}$$

The rate of change of protein mass is proportional to ϕ_R [12], allowing us to define the growth rate of a single cell as $\kappa = \kappa_t(a,U)\phi_R$.

The dynamics of the amino acid mass fraction, a, are given by the difference in the rate of nutrient import and conversion of nutrients to amino acids, and the rate of consumption via translation: $\frac{da}{dt} = \kappa_n(a)\phi_P - \kappa$, where $\kappa_n(a)$ denotes the nutritional efficiency. Using the constraint $\phi_R + \phi_P + \phi_S + \phi_D = \phi_R^{\max}$, this becomes

$$\frac{da}{dt} = \kappa_n(a)\left(\phi_R^{\max} - \phi_R - \phi_S - \phi_D\right) - \kappa_t(a,U)\phi_R. \tag{A4}$$

To make explicit the dependency of the efficiencies, κ_n and κ_t, on a, we define two regulatory functions, $f(a)$ and $g(a)$, as given by Ref. [47]. Specifically, we assume $\kappa_n = \kappa_n^0(c)f(a)$ and $\kappa_t = \kappa_t^0 g(a)$, where κ_t^0 is a constant, and κ_n^0 is a function of the extracellular nutrient concentration c. The regulatory functions are then:

$$f(a) = \frac{1}{1 + (a/a_n)^2}, \tag{A5}$$

$$g(a) = \frac{(a/a_t)^2}{1 + (a/a_t)^2}, \tag{A6}$$

where translation becomes significantly attenuated for amino acid concentrations below a_t, and the amino acid supply flux becomes significantly attenuated by feedback inhibition for a above a_n.

Steady-state transcriptomic analysis reveals that ribosomal sector expression is reduced to allow for stress sector expression [17]. As such, the fraction of total synthesis capacity devoted to ribosomes, f_R, is now a function of both a and U, specifically,

$$f_R(a,U) = \frac{-f'(a)g(a)\left[\phi_R^{\max} - f_S(U)\right]}{-f'(a)g(a) + f(a)g'(a)}. \tag{A7}$$

When $U = 0$, f_R is chosen to maximize translational flux at steady-state, thus maximizing growth rate [42].

APPENDIX B: COMPUTING THE MIC

As stated in the main text, the minimal inhibitory concentration (MIC) is defined in terms of our model as:

$$\text{MIC} \equiv \min b \;\text{ s.t. }\; \max \mathbf{U} \geqslant U_0. \tag{B1}$$

We take the critical threshold U_0 to be constant, allowing Eq. (1) to be rewritten in terms of the normalized concentration, $\tilde{U} = U/U_0$, i.e.,

$$\frac{d\tilde{U}}{dt} = \frac{\alpha}{U_0}\phi_D b - \beta\phi_S\tilde{U} - \tilde{U}\kappa. \tag{B2}$$

Thus, cell death occurs at $\tilde{U} = 1$, and the fitting parameter α/U_0, which represents the normalized damage production rate constant, determines survival.

As a result, we take $U_0 = 1$ and used the normalized dynamics to solve the constrained optimization problem in Eq. (B1). We use a simple line search method, in which an initial guess and jump distance are specified, the trajectory of $\mathbf{U}$ is solved via numerical integration of the coupled ODEs defined in Sec. I, and then the guess and jump distance are updated each iteration based on the following criteria:

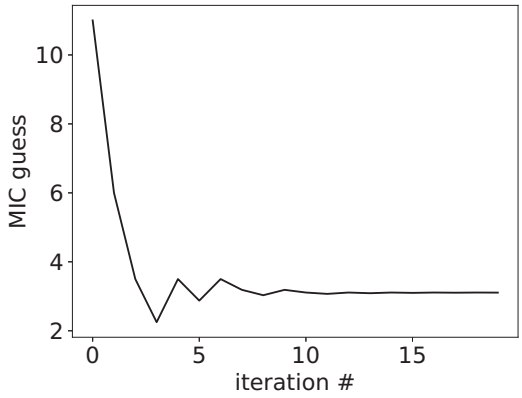

FIG. 7. A simple line search method converges quickly to a solution for the MIC for a given environment.

if $\max \mathbf{U} > U_0$ **then**
  jump $\leftarrow$ jump/2.
  $MIC_{\text{guess}} \leftarrow MIC_{\text{guess}} -$ jump.
else
  $MIC_{\text{guess}} \leftarrow MIC_{\text{guess}} +$ jump.
end if

The algorithm typically converges within ten iterations (Fig. 7).

APPENDIX C: NOTE ON BISTABILITY AND PROTEOME ALLOCATION

Antibiotic-induced growth bistability has been observed experimentally in antibiotic-resistant bacteria [4]. Interestingly, due to the nonlinear nature of target protein expression (ϕ_D) as a function of damage (U), there is a predicted growth bistability in our model in very poor nutrient and high antibiotic environments (Fig. 8, top). The stability of both solutions was confirmed by performing a linear stability analysis of the dynamical equations. In such conditions, faster growing cells carry less damage. Counterintuitively, this fast growth is achieved by reducing ϕ_R and ϕ_D expression, and is not mainly an effect of dilution (Fig. 8, bottom). The increase in translational efficiency caused by the decrease in damage accumulation (caused by reduced target expression) outweighs the decrease in growth caused by reducing ribosomal expression. This bistable behavior is not predicted to occur in any of the environments in which we compare to experimental data.

APPENDIX D: DERIVATION OF RISK OF DEATH

Here we approximate the risk of death as a function of bactericidal antibiotic concentration using Kramer's approximation for our resource allocation and damage

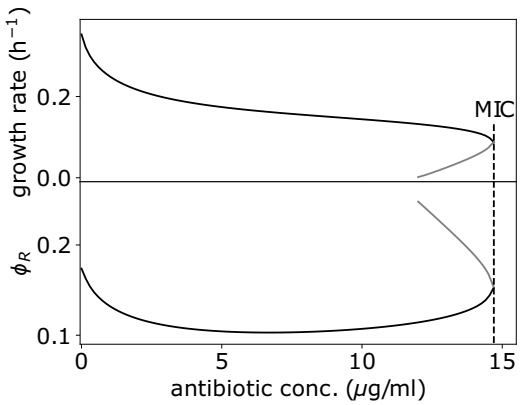

FIG. 8. Predicted growth rate (top) and ribosomal allocation (bottom) bistability. Increased ribosomal expression (gray) corresponds with decreased growth rate (gray).

accumulation model. The model dynamics for damage can be written as:

$$\frac{dU}{dt} = \alpha\phi_D b - \beta\phi_S U - U\kappa + \sqrt{2\sigma}\xi, \tag{D1}$$

where ξ denotes Gaussian white noise. Following Ref. [41], this can be written in terms of a potential function $V(U,t)$:

$$\frac{dU}{dt} = -\frac{\partial V(U,t)}{\partial U} + \sqrt{2\sigma}\xi, \tag{D2}$$

where the potential function is

$$V(U,t) = -\alpha\phi_D(t)bU + \tfrac{1}{2}\{\beta\phi_S(t) + \kappa_t[a(t)]\phi_R(t)\}U^2 - \tfrac{1}{3}\kappa_t[a(t)]\phi_R(t)U^3. \tag{D3}$$

We model mortality as the first time when $U \geqslant 1$ after stepwise application of antibiotic with concentration b. Thus, death time is a first-passage time of U. To estimate the risk of death, i.e., hazard rate, we apply the Kramer approximation [58] for the mean first-passage time:

$$h(t)|_b \approx \frac{\sqrt{V''(U_{ss},t)|V''(1,t)|}}{2\pi}\exp\left(-\frac{V(1,t)-V(U_{ss},t)}{\sigma}\right), \tag{D4}$$

where U_{ss} denotes the quasi steady state of the system at time t after antibiotic application.

In the context of aging, it is usually of interest to calculate the hazard rate and survival function over time [59]. In contrast, here we are interested in understanding how the risk of death changes with increases antibiotic exposure. In this case, a cell is most likely to die when damage is at its maximum value, U^*, which our model predicts will occur shortly after antibiotic application. Thus to estimate the risk of death and survival fraction for a given antibiotic concentration, we define the hazard rate for a given value of b as:

$$\tilde{h}(b) = \max\ h(t)|_b. \tag{D5}$$

Thus using Eqs. (D3), (D4), and (D5), we arrive at an expression for the hazard rate in terms of our model parameters:

$$\tilde{h}(b) = A\exp\left(\frac{\alpha b\phi_D^*(1-U^*) - \tfrac{1}{2}[\beta\phi_S^* + \kappa_t(a^*)\phi_R^*](1-U^{*2}) + \tfrac{1}{3}\kappa_t(a^*)\phi_R^*(1-U^{*3})}{\sigma}\right), \tag{D6}$$

where the prefactor A is given by:

$$A = \sqrt{[\beta\phi_S^* + \kappa_t(a^*)\phi_R^*(1-2U^*)]|\beta\phi_S^* - \kappa_t(a^*)\phi_R^*|}. \tag{D7}$$

Importantly a^*, ϕ_S^*, and ϕ_D^* are the amino acid mass fraction and proteome allocation fractions of the S and D sectors when $U = U^*$, and thus depend on b. Equation (D6) can be solved numerically and is plotted in Fig. 9.

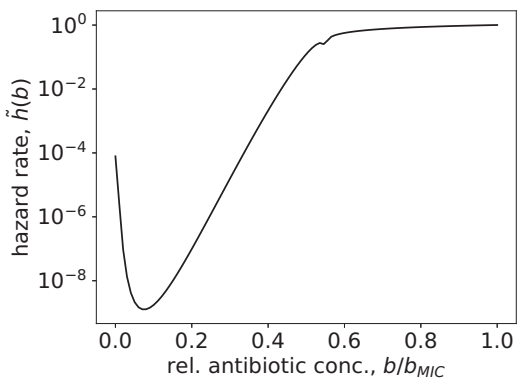

FIG. 9. Maximum hazard rate as a function of applied antibiotic concentration.

This hazard function is related to the survival function, which is the cumulative probability of remaining alive, through the relation:

$$S(b) = \exp\left(-\int_0^b \tilde{h}(B)dB\right). \tag{D8}$$

Equation (D8) can be integrated numerically to predict survival fraction as a function of antibiotic concentration, and can be fit well to experimental data (Fig. 5).

APPENDIX E: PHENOTYPIC SWITCHING MODEL OF POPULATION GROWTH AND DEATH IN PULSATILE ENVIRONMENTS

Here we write a continuum description of population-level growth and death dynamics in response to pulsatile antibiotic exposure. Cells grown in rich media are initially highly susceptible to bactericide application, characterized by a low MIC and high death rate [17]. In response to damage accumulation caused by antibiotics, bacteria alter their gene expression profile, yielding an increase in ϕ_S. As a result, those that survive the initial pulse are better able to with-

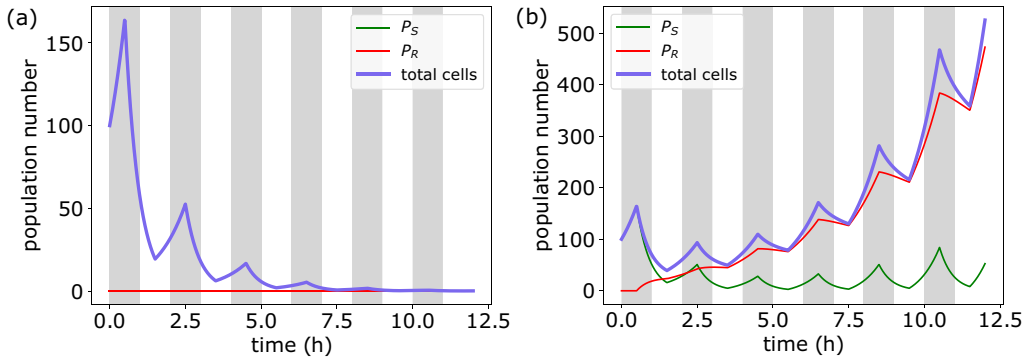

FIG. 10. Population model reproduces adaptation to pulsatile antibiotic exposure seen in our single-cell resource allocation and damage accumulation model. (a) Static population does not survive antibiotic exposure above the MIC. (b) Adaptive population can survive and proliferate by altering its physiological state.

stand subsequent exposure, resulting in an increased MIC and decreased death rate, at the expense of a reduced growth rate. This altering of physiological state can be modeled as a phenotypic switch between two subpopulations, a framework that has been used successfully in pharmacodynamics (PD) to model resistance evolution [50], as well as in modeling bacterial persistence [6]. Critically, unlike previous work, here susceptibility is not altered via mutations or persister formation, but due to changes in gene expression (sector allocation) in growing cells.

PD curves model the effect of drug concentration on net growth rate of bacteria [50]. In the absence of antibiotics, bacteria grow at rate $\kappa_{\max}$, which is set by the nutrient environment. When antibiotics levels are well above the MIC, bacteria are killed at rate $\kappa_{\min}$ ($\kappa_{\min} < 0$). The growth curve for a given nutrient environment can then be defined as [50]:

$$\kappa(b) = \kappa_{\max} - \gamma_i(b), \tag{E1}$$

$$\gamma_i(b) = \frac{(\kappa_{\max} - \kappa_{\min})(b/\mathrm{MIC}_i)^n}{(b/\mathrm{MIC}_i)^n - \kappa_{\min}/\kappa_{\max}}, \tag{E2}$$

where $i = [S, R]$ denotes susceptible cells (P_S) or cells with increased MIC due to an altered physiological state (P_R), with $\mathrm{MIC}_R > \mathrm{MIC}_S$, and where n is the Hill coefficient. We use the notation P_i to stress the fact that they denote two different physiological states of isogenic replicating bacteria. The drug-dependent growth rate can then be used to predict overall population-level dynamics, $P(t)$, from the two subpopulations:

$$\frac{dP_S}{dt} = \{1 - u[b(t-\tau)]\}\kappa_{\max}P_S - \gamma_S[b(t-\tau)]P_S + v[b(t-\tau)](1-c)\kappa_{\max}P_R, \tag{E3}$$

$$\frac{dP_R}{dt} = \{1 - v[b(t-\tau)]\}(1-c)\kappa_{\max}P_R + u[b(t-\tau)]\kappa_{\max}P_S - \gamma_R[b(t-\tau)]P_R, \tag{E4}$$

$$P(t) = P_S(t) + P_R(t), \tag{E5}$$

where $\kappa_{\max}$ is the susceptible bacterial subpopulation maximum net growth rate, and c is the growth cost of altering gene expression to increase resistance. $u(b)$ and $v(b)$ denote the rate of phenotype switching from P_S to P_R, and P_R to P_S, respectively, corresponding to proteome reallocation. For constant antibiotic exposure, this model reduces to a form, which is mathematically equivalent to the Type II persister model presented by Balaban *et al.* [6], however, here we model two subpopulations of growing cells and do not consider the formation of persisters. In Eqs. (E3) and (E4), both $u[b(t-\tau)]$ and $v[b(t-\tau)]$ are functions of the antibiotic concentration with delay τ, such that cells switch from P_S to P_R at rate $u_{\max}$ with some delay in response to antibiotic-induced damage, and switch back from P_R to P_S at rate $v_{\max}$ with some delay when antibiotics are removed to maximize growth. Specifically,

$$u(b-\tau) = u_{\max}\frac{b-\tau}{b_{\max}}, \tag{E6}$$

$$v(b-\tau) = v_{\max}\left(1 - \frac{b-\tau}{b_{\max}}\right). \tag{E7}$$

When antibiotics are pulsed at concentrations above the MIC in a static population, which cannot adapt, the population will perish [Fig. 10(a)]. If surviving cells can alter their physiological state to become more resistant to antibiotics, after several pulses cells are able to adapt and proliferate [Fig. 10(b)]. Critically, this adaptation occurs only when the timescale of returning to the susceptible phenotype (set by $v_{\max}$) is less than the time period of antibiotic pulsing. This population-level description closely matches what is seen in our single-cell simulations (Fig. 6).

[1] R. Roemhild, T. Bollenbach, and D. I. Andersson, The physiology and genetics of bacterial responses to antibiotic combinations, Nat. Rev. Microbiol. **20**, 478 (2022).

[2] K. Mitosch, G. Rieckh, and T. Bollenbach, Noisy response to antibiotic stress predicts subsequent single-cell survival in an acidic environment, Cell Syst. **4**, 393 (2017).

[3] J. M. Blair, M. A. Webber, A. J. Baylay, D. O. Ogbolu, and L. J. Piddock, Molecular mechanisms of antibiotic resistance, Nat. Rev. Microbiol. **13**, 42 (2015).
[4] J. B. Deris, M. Kim, Z. Zhang, H. Okano, R. Hermsen, A. Groisman, and T. Hwa, The innate growth bistability and fitness landscapes of antibiotic-resistant bacteria, Science **342**, 1237435 (2013).
[5] O. Patange, C. Schwall, M. Jones, C. Villava, D. A. Griffith, A. Phillips, and J. C. Locke, *Escherichia coli* can survive stress by noisy growth modulation, Nat. Commun. **9**, 5333 (2018).
[6] N. Q. Balaban, J. Merrin, R. Chait, L. Kowalik, and S. Leibler, Bacterial persistence as a phenotypic switch, Science **305**, 1622 (2004).
[7] B. M. Martins and J. C. Locke, Microbial individuality: How single-cell heterogeneity enables population level strategies, Curr. Opin. Microbiol. **24**, 104 (2015).
[8] J. F. Martin and P. Liras, Organization and expression of genes involved in the biosynthesis of antibiotics and other secondary metabolites, Annu. Rev. Microbiol. **43**, 173 (1989).
[9] S. Sengupta, M. K. Chattopadhyay, and H. P. Grossart, The multifaceted roles of antibiotics and antibiotic resistance in nature, Front. Microbiol. **4**, 1 (2013).
[10] D. I. Andersson and D. Hughes, Microbiological effects of sublethal levels of antibiotics, Nat. Rev. Microbiol. **12**, 465 (2014).
[11] T. Bollenbach, S. Quan, R. Chait, and R. Kishony, Nonoptimal microbial response to antibiotics underlies suppressive drug interactions, Cell **139**, 707 (2009).
[12] M. Scott, C. W. Gunderson, E. M. Mateescu, Z. Zhang, and T. Hwa, Interdependence of cell growth and gene expression: Origins and consequences, Science **330**, 1099 (2010).
[13] P. Greulich, M. Scott, M. R. Evans, and R. J. Allen, Growth-dependent bacterial susceptibility to ribosome-targeting antibiotics, Mol. Syst. Biol. **11**, 796 (2015).
[14] G. Brandis, J. Larsson, and J. Elf, Antibiotic perseverance increases the risk of resistance development, Proc. Natl. Acad. Sci. USA **120**, e2216216120 (2023).
[15] A. C. Palmer, R. Chait, and R. Kishony, Nonoptimal gene expression creates latent potential for antibiotic resistance, Mol. Biol. Evol. **35**, 2669 (2018).
[16] M. Mori, Z. Zhang, A. BanaeiEsfahani, J. Lalanne, H. Okano, B. C. Collins, A. Schmidt, O. T. Schubert, D. Lee, G. Li, R. Aebersold, T. Hwa, and C. Ludwig, From coarse to fine: The absolute *Escherichia coli* proteome under diverse growth conditions, Mol. Syst. Biol. **17**, e9536 (2021).
[17] A. Bren, D. S. Glass, Y. K. Kohanim, A. Mayo, and U. Alon, Tradeoffs in bacterial physiology determine the efficiency of antibiotic killing, Proc. Natl. Acad. Sci. USA **120**, e2312651120 (2023).
[18] P. Nonejuie, M. Burkart, K. Pogliano, and J. Pogliano, Bacterial cytological profiling rapidly identifies the cellular pathways targeted by antibacterial molecules, Proc. Natl. Acad. Sci. USA **110**, 16169 (2013).
[19] L. K. Harris and J. A. Theriot, Relative rates of surface and volume synthesis set bacterial cell size, Cell **165**, 1479 (2016).
[20] C. Cylke, F. Si, and S. Banerjee, Effects of antibiotics on bacterial cell morphology and their physiological origins, Biochem. Soc. Trans. **50**, 1269 (2022).
[21] N. Ojkic, D. Serbanescu, and S. Banerjee, Antibiotic resistance via bacterial cell shape-shifting, mBio **13**, e00659-22 (2022).
[22] F. Baquero and B. R. Levin, Proximate and ultimate causes of the bactericidal action of antibiotics, Nat. Rev. Microbiol. **19**, 123 (2021).
[23] E. Tuomanen, R. Cozens, W. Tosch, and A. Tomasz, The rate of killing of *Escherichia coli* by B-lactam antibiotics is strictly proportional to the rate of bacterial growth, J. Gen. Microbiol. **132**, 1297 (1986).
[24] G. V. Smirnova and O. N. Oktyabrsky, Relationship between *Escherichia coli* growth rate and bacterial susceptibility to ciprofloxacin, FEMS Microbiol. Lett. **365**, 1 (2018).
[25] A. J. Lopatkin, J. M. Stokes, E. J. Zheng, J. H. Yang, M. K. Takahashi, L. You, and J. J. Collins, Bacterial metabolic state more accurately predicts antibiotic lethality than growth rate, Nat. Microbiol. **4**, 2109 (2019).
[26] A. Y. Weiße, D. A. Oyarzún, V. Danos, and P. S. Swain, Mechanistic links between cellular trade-offs, gene expression, and growth, Proc. Natl. Acad. Sci. USA **112**, E1038 (2015).
[27] D. Serbanescu, N. Ojkic, and S. Banerjee, Nutrient-dependent trade-offs between ribosomes and division protein synthesis control bacterial cell size and growth, Cell Rep. **32**, 108183 (2020).
[28] N. Ojkic, E. Lilja, S. Direito, A. Dawson, R. J. Allen, and B. Waclaw, A Roadblock-and-Kill mechanism of action model for the dna-targeting antibiotic ciprofloxacin, Antimicrob. Agents Chemo. **64**, e02487-19 (2020).
[29] See Supplemental Material at http://link.aps.org/supplemental/10.1103/PRXLife.2.013010 for Supplemental Figs. S1 (data analysis showing coregulation of quinolone targets with R-sector), S2 (growth rate dynamics during antibiotic pulse), S3 (bimodal growth rate distribution), S4 (resouce allocation in pulsatile environment), S5 and S6 (parameter variation).
[30] B. D. Towbin, Y. Korem, A. Bren, S. Doron, R. Sorek, and U. Alon, Optimality and sub-optimality in a bacterial growth law, Nat. Commun. **8**, 14123 (2017).
[31] X. P. Hu, H. Dourado, P. Schubert, and M. J. Lercher, The protein translation machinery is expressed for maximal efficiency in *Escherichia coli*, Nat. Commun. **11**, 1 (2020).
[32] J. S. Edwards, R. U. Ibarra, and B. O. Palsson, In silico predictions of *Escherichia coli* metabolic capabilities are consistent with experimental data, Nat. Biotechnol. **19**, 125 (2001).
[33] M. A. Kohanski, D. J. Dwyer, B. Hayete, C. A. Lawrence, and J. J. Collins, A common mechanism of cellular death induced by bactericidal antibiotics, Cell **130**, 797 (2007).
[34] P. Belenky, J. D. Ye, C. B. Porter, N. R. Cohen, M. A. Lobritz, T. Ferrante, S. Jain, B. J. Korry, E. G. Schwarz, G. C. Walker, and J. J. Collins, Bactericidal antibiotics induce toxic metabolic perturbations that lead to cellular damage, Cell Rep. **13**, 968 (2015).
[35] D. J. Dwyer, M. A. Kohanski, B. Hayete, and J. J. Collins, Gyrase inhibitors induce an oxidative damage cellular death pathway in *Escherichia coli*, Mol. Syst. Biol. **3**, 91 (2007).
[36] D. J. Dwyer, P. A. Belenky, J. H. Yang, I. Cody MacDonald, J. D. Martell, N. Takahashi, C. T. Chan, M. A. Lobritz, D. Braff, E. G. Schwarz, J. D. Ye, M. Pati, M. Vercruysse, P. S. Ralifo, K. R. Allison, A. S. Khalil, A. Y. Ting, G. C. Walker, and J. J. Collins, Antibiotics induce redox-related physiological alterations as part of their lethality, Proc. Natl. Acad. Sci. USA **111**, (2014).
[37] A. M. Brauer, H. Shi, P. A. Levin, and K. C. Huang, Physiological and regulatory convergence between osmotic and nutrient

stress responses in microbes, Curr. Opin. Cell Biol. **81**, 102170 (2023).

[38] K. Kvint, L. Nachin, A. Diez, and T. Nyström, The bacterial universal stress protein: Function and regulation, Curr. Opin. Microbiol. **6**, 140 (2003).

[39] J. Coates, B. R. Park, D. Le, E. Şimşek, W. Chaudhry, and M. Kim, Antibiotic-induced population fluctuations and stochastic clearance of bacteria, eLife **7**, e32976 (2018).

[40] K. J. Aldred, R. J. Kerns, and N. Osheroff, Mechanism of quinolone action and resistance, Biochem. **53**, 1565 (2014).

[41] Y. Yang, O. Karin, A. Mayo, X. Song, P. Chen, A. L. Santos, A. B. Lindner, and U. Alon, Damage dynamics and the role of chance in the timing of *E. coli* cell death, Nat. Commun. **14**, 1 (2023).

[42] J. C. Kratz and S. Banerjee, Dynamic proteome trade-offs regulate bacterial cell size and growth in fluctuating nutrient environments, Commun. Biol. **6**, 486 (2023).

[43] S. Hui, J. M. Silverman, S. S. Chen, D. W. Erickson, M. Basan, J. Wang, T. Hwa, and J. R. Williamson, Quantitative proteomic analysis reveals a simple strategy of global resource allocation in bacteria, Mol. Syst. Biol. **11**, 784 (2015).

[44] P. Sanchez-Vazquez, C. N. Dewey, N. Kitten, W. Ross, and R. L. Gourse, Genome-wide effects on *Escherichia coli* transcription from ppGpp binding to its two sites on RNA polymerase, Proc. Natl. Acad. Sci. USA **116**, 8310 (2019).

[45] A. Battesti, N. Majdalani, and S. Gottesman, The RpoS-mediated general stress response in *Escherichia coli*, Annu. Rev. Microbiol. **65**, 189 (2011).

[46] D. Molenaar, R. Van Berlo, D. De Ridder, and B. Teusink, Shifts in growth strategies reflect tradeoffs in cellular economics, Mol. Syst. Biol. **5**, 323 (2009).

[47] M. Scott, S. Klumpp, E. M. Mateescu, and T. Hwa, Emergence of robust growth laws from optimal regulation of ribosome synthesis, Mol. Syst. Biol. **10**, 747 (2014).

[48] H. Teimouri and A. B. Kolomeisky, Theoretical investigation of stochastic clearance of bacteria: First-passage analysis, J. R. Soc. Interface **16**, 20180765 (2019).

[49] R. Mathis and M. Ackermann, Asymmetric cellular memory in bacteria exposed to antibiotics, BMC Evol. Biol. **17**, 73 (2017).

[50] C. Witzany, J. Rolff, R. Regoes, and C. Igler, The pharmacokinetic-pharmacodynamic modeling framework as a tool to predict drug resistance evolution, Microbiol. **169**, 001368 (2023).

[51] A. Brauner, O. Fridman, O. Gefen, and N. Q. Balaban, Distinguishing between resistance, tolerance and persistence to antibiotic treatment, Nat. Rev. Microbiol. **14**, 320 (2016).

[52] F. Abram, T. Arcari, D. Guerreiro, and C. P. O'Byrne, Evolutionary trade-offs between growth and survival: The delicate balance between reproductive success and longevity in bacteria, Adv. Microbial Physiol. **79**, 133 (2021).

[53] P. H. Plotz and B. D. Davis, Synergism between streptomycin and penicillin: A proposed mechanism, Science **135**, 1067 (1962).

[54] R. Roemhild, C. S. Gokhale, P. Dirksen, C. Blake, P. Rosenstiel, A. Traulsen, D. I. Andersson, and H. Schulenburg, Cellular hysteresis as a principle to maximize the efficacy of antibiotic therapy, Proc. Natl. Acad. Sci. USA **115**, 9767 (2018).

[55] E. Martínez-Salas, J. A. Martin, and M. Vicente, Relationship of *Escherichia coli* density to growth rate and cell age, J. Bacteriol. **147**, 97 (1981).

[56] N. M. Belliveau, G. Chure, C. L. Hueschen, H. G. Garcia, J. Kondev, D. S. Fisher, J. A. Theriot, and R. Phillips, Fundamental limits on the rate of bacterial growth and their influence on proteomic composition, Cell Syst. **12**, 924 (2021).

[57] M. A. Borovinskaya, R. D. Pai, W. Zhang, B. S. Schuwirth, J. M. Holton, G. Hirokawa, H. Kaji, A. Kaji, and J. H. Cate, Structural basis for aminoglycoside inhibition of bacterial ribosome recycling, Nat. Struct. Mol. Biol. **14**, 727 (2007).

[58] N. Berglund, Kramers' law: Validity, derivations and generalisations, Markov Processes Relat. Fields **19**, 459 (2013).

[59] N. Stroustrup, Measuring and modeling interventions in aging, Curr. Opin. Cell Biol. **55**, 129 (2018).